based polymers; see, e.g. (*29*) or (*30*). However, the origin of this difference is controversial and may depend on photooxidation of the sample or the intensity of the excitation beam in addition to interchain effects; see, e.g. (*30*–*32*). No matter how the effect arises, under the conditions of our experiments, the decay of MEH-PPV's excited state absorption is different in solution and film environments (Fig. 2). Thus, we can use excited state absorption to help determine the local environment of the polymer in different regions of the composite sample.

29. M. Yan, L. J. Rothberg, E. W. Kwock, T. M. Miller, *Phys. Rev. Lett.* **75**, 1992 (1995).
30. T.-Q. Nguyen, I. Martini, J. Liu, B. J. Schwartz, *J. Phys. Chem. B* **104**, 237 (2000).
31. N. T. Harrison, G. R. Hayes, R. T. Phillips, R. H. Friend, *Phys. Rev. Lett.* **77**, 1881 (1996).
32. V. I. Klimov, D. W. McBranch, N. N. Barashkov, J. P. Ferraris, *Chem. Phys. Lett.* **277**, 109 (1997).
33. The polarization notation used throughout this report is as follows: the first character indicates the pore direction in the lab frame (always vertical in this report), the second character indicates the lab polarization of the excitation beam, and the third character denotes the collection or probe polarization direction. For example, VHV indicates excitation light polarized perpendicular to the pore direction but collection or probe light polarized along the pore channels.
34. C. R. Cantor and P. R. Schimel, *Biophysical Chemistry, Part II* (Freeman, San Francisco, CA, 1980), p. 474.
35. The single exponential fit is not representative of a particular model for intrachain energy transport; rather, it is merely a way to define a characteristic time for the anisotropy increase. Because the anisotropy at long times is computed from the ratio of two small numbers (Eq. 1 at times after most of the excitons have decayed), we do not feel that the signal-to-noise ratio of the anisotropy increase justifies fitting to a more complex model with a higher number of parameters.
36. C. Weder, C. Sarwa, C. Bastiaansen, P. Smith, *Adv. Mater.* **9**, 1035 (1997).
37. G. R. Hayes, I. D. W. Samuel, R. T. Phillips, *Phys. Rev. B* **56**, 3838 (1997).
38. A. Watanabe, T. Kodaira, O. Ito, *Chem. Phys. Lett.* **273**, 227 (1997).
39. A. Ruseckas *et al., J. Lumin.* **76-77**, 474 (1998).
40. J. Z. Zhang *et al., J. Chem. Phys.* **106**, 3710 (1997).
41. R. J. O. M. Hoofman, M. P. deHaas, L. D. A. Siebbeles, J. M. Warman, *Nature* **392**, 54 (1998).
42. Supported by the Petroleum Research Fund, administered by the ACS (grants 32773-G6 and 33715-G5); the Office of Naval Research (grant N00014-99-1-0568); the NSF (grant DMR-9971842). B.J.S. is a Cottrell Scholar of Research Corporation and an Alfred P. Sloan Foundation Research Fellow. We thank F. Wudl and R. Helgeson for providing the MEH-PPV used in this work.

2 September 1999; accepted 2 March 2000

A Superconducting Field-Effect Switch

J. H. Schön,[1] Ch. Kloc,[1] R. C. Haddon,[2] B. Batlogg[1]

We report here on a novel realization of a field-effect device that allows switching between insulating and superconducting states, which is the widest possible variation of electrical properties of a material. We chose C_{60} as the active material because of its low surface state density and observed superconductivity in alkali metal–doped C_{60}. We induced three electrons per C_{60} molecule in the topmost molecular layer of a crystal with the field-effect device, creating a superconducting switch operating up to 11 kelvin. An insulator was thereby transformed into a superconductor. This technique offers new opportunities for the study of superconductivity as a function of carrier concentration.

The basic idea of an ideal electric "valve" goes back to the late 1920s and involves switching between high- and low-resistance regimes by an applied electric field (*1*). However, reliable devices could not be prepared until 30 years later (*2*), surface states of inorganic semiconductors, such as silicon or germanium, being the major hurdle. Since then, the silicon field-effect transistor (FET) has become the cornerstone of modern semiconductor industry and technology. In addition, there has been an ongoing effort to modulate superconductivity in thin films by an applied static electric field (*3*). Shifts of the transition temperature T_c of up to 30 K have been observed in high-T_c cuprate films, caused by changing the concentration of charge carriers in the electronically active CuO_2 layers (*4, 5*). However, complete field-induced switching between superconducting and insulating states remains a desirable goal. Here we report on a novel C_{60}-based field-effect device, an ultimate switch between the insulating and superconducting regimes of chemically pure C_{60}.

Working with C_{60} as the starting material is advantageous because so much is known about transport, and ultimately superconductivity, in C_{60} when electrons are induced by chemical doping (*6, 7*). Undoped C_{60} has a band gap of approximately 2 eV and is therefore insulating, whereas alkali metal–doped C_{60} (A_3C_{60}) exhibits metallic conductivity and, at low temperatures, superconductivity. Furthermore, working with van der Waals–bonded materials, such as molecular crystals, offers the inherent advantage of low surface state densities because of the absence of dangling bond–type surface states. Previous studies on organic semiconductors such as pentacene have shown that in an organic FET the chemical potential can be shifted easily across the band gap of the semiconductor, leading to *n*- as well as *p*-channel activity (*8*).

We have grown C_{60} single crystals that are several mm^3 in size in a stream of hydrogen in an apparatus similar to that used for the growth of other organic semiconductor crystals (*9*). Multiply sublimed material was used as a starting material. In order to prepare field-effect devices on C_{60} single crystals, we evaporated gold source and drain contacts on smooth growth surfaces through a shadow mask. Channels were typically 25 to 50 μm long and 500 to 1000 μm wide. Sputtered Al_2O_3 with a capacitance C_i of 185 nF/cm^2 was used as the gate dielectric. Finally, a gold gate electrode was deposited on top of the oxide (Fig. 1). FET measurements were carried out in vacuum at temperatures between 4 and 300 K. Additional space charge–limited current measurements were used to determine the number of electrically active defects in these high-quality single crystals (*10*). Trap concentrations (deep levels) as low as 3×10^{12} cm^{-3} (one per 5×10^8 C_{60} molecules) are estimated. This level is significantly lower than those reported earlier for other vacuum-grown crystals (*11*).

Previous thin film C_{60} transistors exhibited *n*-type behavior and field-effect mobilities of 0.09 cm^2/V·s (*12*). Figure 1 shows the typical transistor characteristics at room temperature for single-crystal devices. These devices show *n*- as well as *p*-channel activity, reflecting the ambipolar transport in these high-quality single crystals and further emphasizing the low interface state density of the FET. Electron and hole mobilities of 2.1 and 1.8 cm^2/V·s, respectively, are deduced from standard semiconductor equations (*13*). At room temperature, the channel resistance can be varied over approximately nine orders of magnitude by the applied gate bias (Fig. 2A). Figure 2A shows the channel resistance as a function of gate charge ($n = C_iV_g/e$, where n is the charge carrier density, C_i is the capacitance, V_g is the gate voltage, and e is the elementary charge) at room temperature and 5 K. The initial drop of the resistance at a few volts reflects the turn-on of the FET. At larger bias, charge accumulates in the channel, leading to a gradual decrease of the resistance. Finally, at very high positive gate voltages, the channel resistance drops abruptly to zero below a critical temperature T_c of 11 K. The channel evidently becomes superconducting. The drop of the resistance depends both on the applied gate voltage and on the temperature. This is shown in Fig. 2B, where the channel resistance is plotted versus temperature and the gate charge. A priori we do not know the electronic nature of the superconducting channel; that is, how many molecular layers become supercon-

[1]Bell Laboratories, Lucent Technologies, 600 Mountain Avenue, Murray Hill, NJ 07974, USA. [2]Departments of Chemistry and Physics and Advanced Carbon Materials Center, University of Kentucky, Lexington, KY 40506, USA.

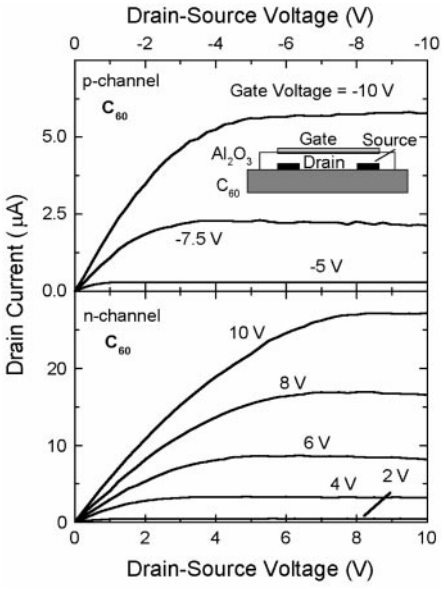

Fig. 1. Source-drain current versus gate voltage at room temperature for a C_{60} single-crystal FET. Top, *p*-channel operation; bottom, *n*-channel operation. The inset shows the schematic structure of a single-crystal FET.

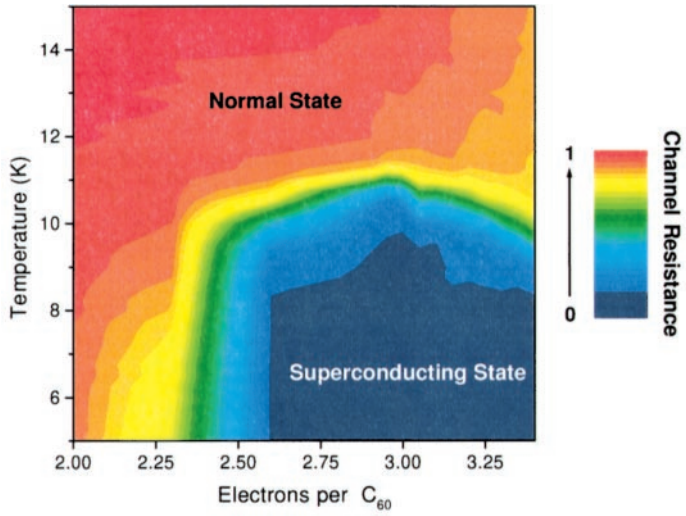

Fig. 3. Channel resistance as a function of temperature and electrons per C_{60} molecule. The electron concentration is calculated assuming that only the first molecular layer accepts charge. The maximum of the transition temperature at three electrons per molecule is in accordance with measurements on chemically doped A_3C_{60} (red, normal state; blue, superconducting state).

ducting. However, excellent agreement with known bulk superconductivity in A_3C_{60} (*14*) is found if we assume that only a single layer of C_{60} molecules accepts the electrons (*15*). The area density is approximately 9×10^{13} C_{60} molecules per cm^2 and the gate charge corresponds to 2.7×10^{13} electrons per cm^2, which is equivalent to three electrons per molecule (C_{60}^{3-}). In bulk A_xC_{60}, this carrier concentration is known to produce the optimum T_c, as the Fermi level lies near the maximum in the density of states of the conduction band. A more detailed map of the superconducting T_c as function of gate bias, expressed in terms of electrons per C_{60}, is shown in Fig. 3. The critical temperature is maximal for three electrons per C_{60} molecule (*14*). Hence, we conclude that field-induced doping results in the same superconducting phenomena as does chemical doping in bulk A_3C_{60}.

Modifying the lattice constant of A_3C_{60} by doping or pressure results in a change of the lattice constant and of the electronic bandwidth, and therefore of the density of states at the Fermi level. Consequently, T_c varies in accordance with Bardeen-Cooper-Schrieffer theory (*6, 16, 17*). A systematic variation of T_c with the lattice constant is indeed observed for A_xC_{60} (slight deviations from the cubic crystal structure are ignored here). The value of $T_c = 11$ K observed in our field-effect switch is slightly lower ($\approx$3 to 4 K) than expected from the "universal curve" (Fig. 4). This T_c reduction might be ascribed to the two-dimensional nature of the channel region as compared to the three-dimensional properties of bulk samples (*15*).

A first characterization of the superconducting channel involves the upper critical magnetic field H_{c2} (Fig. 5). The slope of the critical field (dH_{c2}/dT) is approximately -5 T/K in the range reported for bulk A_3C_{60} (*6*). Using the standard extrapolation to $T = 0$ K, we can estimate the coherence length to be on the order of 30 Å. This is further evidence that superconductivity in a C_{60} field-effect device is of the

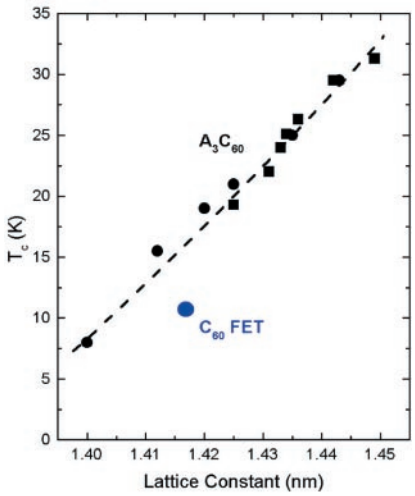

Fig. 4. Transition temperature for bulk alkali-doped A_3C_{60} and our C_{60} field-effect switch. The values for A_3C_{60} are taken from (*6*).

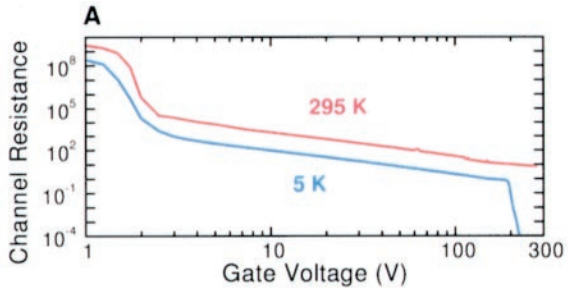

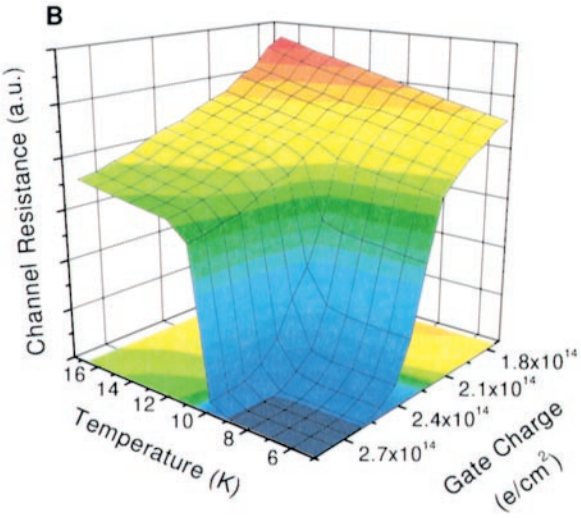

Fig. 2. Channel resistance of a C_{60} single-crystal FET as a function of applied gate voltage and temperature. (**A**) Resistance at 5 K and room temperature as a function of gate voltage. The transition to the superconducting state is seen as a drop in the blue curve. (**B**) Resistance as a function of gate charge (C_iV_g) and temperature, demonstrating superconductivity for concentration above 2.5×10^{14} cm^{-2} and below $T_c = 11$ K.

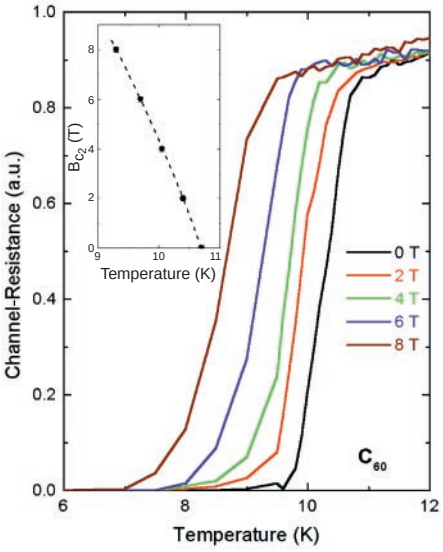

Fig. 5. Transition to the superconducting state for different magnetic fields applied perpendicular to the channel. The variation of the upper critical magnetic field H_{c2} with temperature is shown in the inset (slope ≈ -5 T/K).

same type as in A_3C_{60}. The filling of the band is controlled by the applied gate voltage, and because of the strong electron-phonon interaction in this material, the channel region becomes superconducting below 11 K.

The possibility of investigating superconductivity as function of electron (or hole) density in a simple FET device opens up various opportunities to find superconductivity in new classes of materials, especially organic semiconductors. In addition to being able to implement the longstanding idea of an ultimate field-induced switch (insulator-superconductor transformation), this technique also opens up new ways to substantially modify the electronic state in molecular crystals.

References and Notes

1. J. E. Lilienfeld, U.S. Patent 1,745,175 (1926).
2. M. M. Atalla, E. Tennenbaum, E. J. Scheiber, *Bell Syst. Tech. J.* **28**, 749 (1959).
3. R. E. Glover and M. D. Sherill, *Phys. Rev. Lett.* **5**, 248 (1960).
4. J. Mannhart, J. Ströbel, J. G. Bednorz, Ch. Gerber, *Appl. Phys. Lett.* **62**, 630 (1993).
5. J. Mannhart, J. G. Bednorz, K. A. Müller, D. G. Schlom, J. Ströbel, *J. Alloys Compd.* **195**, 519 (1993).
6. M. S. Dresselhaus, G. Dresselhaus, R. Saito, in *Physical Properties of High Temperature Superconductors IV*, D. M. Ginsberg, Ed. (World Scientific, Singapore, 1994), pp. 471–565; A. P. Ramirez, *Supercond. Rev.* **1**, 1 (1994).
7. A. F. Hebard *et al.*, *Nature* **350**, 600 (1991).
8. J. H. Schön, S. Berg, Ch. Kloc, B. Batlogg, *Science* **287**, 1022 (2000).
9. Ch. Kloc, P. G. Simpkins, T. Siegrist, R. A. Laudise, *J. Cryst. Growth* **182**, 416 (1997).
10. J. H. Schön, Ch. Kloc, R. A. Laudise, B. Batlogg, *Phys. Rev. B* **58**, 12952 (1998).
11. E. Frankevich, Y. Maruyama, H. Ogata, *Chem. Phys. Lett.* **214**, 39 (1993).
12. R. C. Haddon *et al.*, *Appl. Phys. Lett.* **67**, 121 (1995).
13. S. M. Sze, *Physics of Semiconductor Devices* (Wiley, New York, 1981).
14. T. Yildirim *et al.*, *Phys. Rev. Lett.* **77**, 167 (1996).
15. It has been observed that the charge transfer across a copper/C_{60} interface also occurs only at the topmost layer of C_{60} [A. F. Hebard, R. R. Ruel, C. B. Eom, *Phys. Rev. B* **54**, 14052 (1996)].
16. C. M. Varma, J. Zaanen, K. Raghavachari, *Science* **254**, 989 (1991).
17. M. A. Schlüter, M. Lannoo, M. Needls, G. A. Baraff, D. Tomanek, *Phys. Rev. Lett.* **68**, 526 (1992).

18. J.H.S. gratefully acknowledges financial support by the Deutsche Forschungsgemeinschaft. We thank E. Bucher for the use of equipment and H. Y. Hwang, D. W. Murphy, H. Störmer, and C. M. Varma for helpful discussions.

6 March 2000; accepted 6 April 2000

The Archean Sulfur Cycle and the Early History of Atmospheric Oxygen

Donald E. Canfield,* Kirsten S. Habicht, Bo Thamdrup

The isotope record of sedimentary sulfides can help resolve the history of oxygen accumulation into the atmosphere. We measured sulfur isotopic fractionation during microbial sulfate reduction up to 88°C and show how sulfate reduction rate influences the preservation of biological fractionations in sediments. The sedimentary sulfur isotope record suggests low concentrations of seawater sulfate and atmospheric oxygen in the early Archean (3.4 to 2.8 billion years ago). The accumulation of oxygen and sulfate began later, in the early Proterozoic (2.5 to 0.54 billion years ago).

Life has dramatically modified the surface chemistry of Earth. A most conspicuous expression of this is the accumulation of oxygen, a product of oxygenic photosynthesis by plants and cyanobacteria, into the atmosphere and oceans. Atmospheric oxygen promotes the oxidative weathering of rocks on land, forming oxidized species such as iron oxides and soluble sulfate (*1*). As a result, the accumulation of sulfate into the oceans (the concentration is presently 28 mM) and the formation of iron oxides during weathering on land are two substantial geochemical expressions of oxygen accumulation into the atmosphere (*1*, *2*). Still, considerable controversy and debate surround when atmospheric oxygen first began to accumulate. In one scenario, atmospheric oxygen reached present-day levels by the earliest Archean [3.8 billion years ago (Ga)] and has persisted in high concentrations ever since (*3*). In another scenario, atmospheric oxygen first began to accumulate much later, around 2.2 to 2.3 Ga in the early Proterozoic (*2*). Present-day levels may not have been reached until sometime in the Neoproterozoic, 0.54 to 1.0 Ga (*4*).

The history of seawater sulfate concentrations is germane to differentiating between these two models for atmospheric oxygen accumulation. Low concentrations of seawater sulfate into the early Archean would be consistent with, and provide evidence for, low early Archean concentrations of atmospheric oxygen (*5*). Inferences as to the history of seawater sulfate accumulation are based, primarily, on interpretations of the sulfur isotope record of ancient sedimentary sulfide minerals. This record shows sedimentary sulfides between 3.4 and 2.8 Ga with isotopic compositions of ±5 per mil (‰) around a contemporaneous seawater sulfate isotopic composition [$\delta^{34}S$ (*6*)] of 2 to 3‰ (*7*). The principal feature of this record is the small isotope difference between seawater sulfate and sedimentary sulfides.

The interpretation of this record is based on our understanding of the factors controlling isotope fractionation during sulfate reduction by sulfate-reducing bacteria. These bacteria are responsible for most of the sulfide formed in modern marine sediments. There is a tendency for pure cultures of sulfate-reducing bacteria to fractionate less as specific rates (rate per cell) of sulfate reduction increase (*8*). Increasing temperature can lead to higher specific rates for individual species of sulfate reducers, and, therefore, lower fractionations might be expected at higher temperatures. Thus, minimally fractionated early Archean sedimentary sulfides may have formed at rapid rates of sulfate reduction in a warm, sulfate-rich (10 to 28 mM) ocean (*3*, *9*), providing support for high early Archean atmospheric oxygen concentrations (*3*, *9*).

This ocean model requires extensions of relations between specific rates of sulfate reduction, temperature, and isotope fractionation beyond current observations. Thus, for *Desulfovibrio desulfuricans*, the most studied sulfate-reducing bacterium, fractionations of 10 to 26‰ are observed at 40° to 45°C, the upper temperature limit for the survival of the organism, where specific rates of sulfate reduc-

Danish Center for Earth System Science (DCESS) and Institute of Biology, Odense University, SDU, Campusvej 55, 5230 Odense M, Denmark.

*To whom correspondence should be addressed. E-mail: dec@biology.ou.dk